2/18/09

ECS line fluxes and illumination pattern from the Ball dataset

A.Vikhlinin

Abstract

This memo presents a report on the measurements performed using the ground ACIS ECS data:

1. Average energy for the L-shell complex
2. Pre-flight ratio of the Mn L and K line fluxes
3. Cross-calibration of the S3 ad S2 quantum efficiency
4. ACIS illumination pattern from the main lines

1 Data and reduction

The data were provided by C. Grant. It was cleaned from the bad ASCA grades. Exposures were calculated by Catherine by counting the frames.

The additional reductions applied are:

1. In each node, calculate the locations for the Al-Ka, Ti-Ka, and Mn-Ka lines. The algorithm for line centroid is a) identify the peak; b) measure FWHM; c) measure the mean location using a window of FWHM channels
   ```
   ./mk_locations
   ```
2. fit linear gain coefficients
   ```
   ./fit_lin_gain gais.dat >! gain_fit.dat
   ```
3. Apply linear gains using `pha_pi` and the standard gain to S3 and S1
   ```
   ./pha_pi ball_i?.fits ball_s2.fits ball_s4.fits
   apply_gain ball_s[31].fits -gain $CH/CAL/gain.fits
   ```
4. Detect and remove extra bad pixels
   ```
   rename -exe ball_*.fits epoch-100_*.fits
   ../process/find_bad_pix -100 > bad.pix.list
   ../process/rm_bad_pixels -100
   rename -exe epoch-100_*.fits ball_*.fits
   ```
5. Extract spectra for the entire chips
   ```
   ./extr_spectra_chip
   ```
6. Response matrix for the FI chips is calculated with the CTI scatter turned off and the pre-cti response narrowed by a factor of 0.925. The S3 rmf is computed with a slightly scaled CTI matrix:
   ```
   calcrmf2 -phafile cs3_0.pha -o fi.rmf @../bin.contamination/par.file \
       ccd_id=3 updateheader=no scalectimatr=0.1 scale_precti_rmf=0.925
   calcrmf2 -phafile s3.pha -o bi.rmf @par.file ccd_id=7 scalectimatr=0.9
   calcrmf2 -phafile s1.pha -o s1.rmf @par.file ccd_id=5
   ```

2 Average Energy of the L-shell Complex

Purpose: The ratio of the line intensities in the ECS L-complex can be important for normalizing the optical depths of the contamination on the ACIS OBF. Unfortunately, the L-complex is unresolved. The relative line intensities can be deduced from the average energy of the L-complex because we know the nominal energies for the Fe and Mn L-lines. The FI CCDs are best-suited for this measurements because on the ground, their gain was linear and the energy resolution was much better than in the BI CCDs.

Measurements: The data in the 0.4–1.2 keV range is fit with a single gaussian (free width) plus the exponential tail to represent the tail of the Al-Ka line plus a power law to represent the background (e.g., Fig. 1). The results are reported in Table 1. The average energy of the L-complex is measured to be 0.665 ± 0.001 keV.

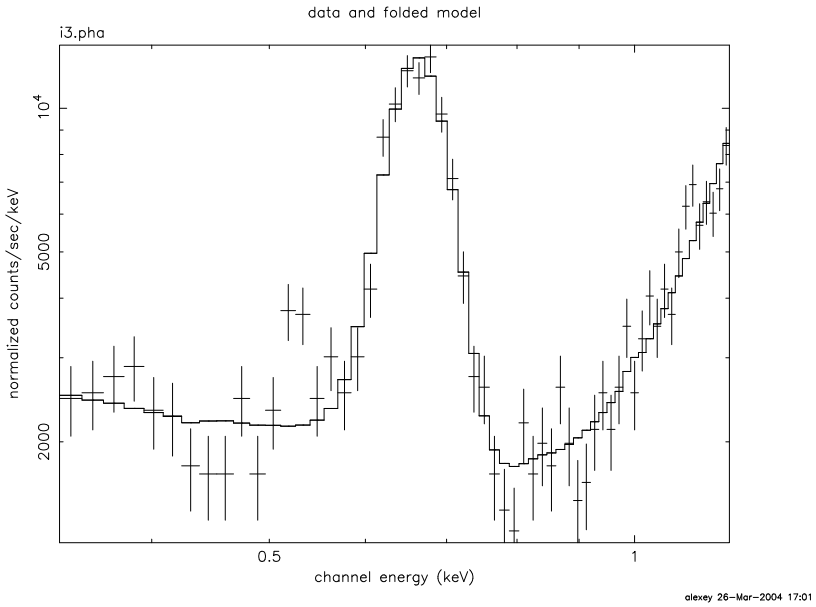

Fig. 1— Example of the L-complex fit with a single Gaussian (I3).

Table 1— L-complex centroids in the FI chips

CCD	$\langle E\rangle_L$, keV
I0	0.669 ± 0.003
I1	0.663 ± 0.002
I2	0.667 ± 0.003
I3	0.664 ± 0.002
S2	0.662 ± 0.002
Average	0.665 ± 0.001

Table 2— Expected energies are relative intensities of the L-complex lines (from H. Marshall)

Transition	Fraction	E(Fe)	E(Mn)
L-$\alpha_{1,2}$	0.836	0.7050	0.6374
L-β_1	0.077	0.7185	0.6488
L-ζ	0.068	0.6152	0.5563
L-η	0.019	0.6280	0.5675

Expected energy of the L-complex: Herman Marshall provided the line energies and relative intensities for the Mn- and Fe-L lines. The line energies were obtained from the paper by Bearden (1967, Rev.Mod.Phy. 39, p. 121), and relative intensities are for the Cu EIPS anode HETG calibration from XRCF. Marshall's results are listed in Table 2.

It is clear from Fig. 1 that the line complex at 0.56 keV (Mn-Lζ,η) should be well separated from the main peak and thus does not contribute to the measurement of the average energy of the L-complex. The rest of the lines are confused.

To simplify the normalization of the contamination optical depth, it is convenient to combine the lines into 3 groups:

$$\langle E\rangle_{\mathrm{Fe}\ \alpha,\beta} = 0.706\,\mathrm{keV} \qquad \langle E\rangle_{\mathrm{Mn}\ \alpha,\beta} = 0.638\,\mathrm{keV} \qquad \langle E\rangle_{\mathrm{Fe}\ \zeta,\eta} = 0.618\,\mathrm{keV}. \tag{1}$$

The expected ratio of the fluxes in Fe α,β and Fe ζ,η is 0.913 : 0.087. However, the effective area of the FI chips drops significantly, by a factor of 1.60, between 0.706 and 0.618 keV (see Table 3 below); therefore, the expected count rate ratio is 0.944 : 0.056. If X is the count rate fraction in Fe lines, we can write the average energy of the L-complex as

$$\langle E\rangle = 0.706\times 0.944\times X + 0.638\times(1-X) + 0.618\times 0.056\times X = 0.063\,X + 0.638. \tag{2}$$

Results: Using the measurement $\langle E\rangle = 0.665$, we obtain **X = 0.43**. Therefore, the L-complex in the FI chips should consist of 57% in the Mn α,β lines, 40.6% in Fe α,β, and 2.4% in Fe ζ,η.

The precise measurements of the L-complex energy in the BI chips are difficult because of the non-linear gain. Instead, we can use the ratio of the nominal QE in the BI and FI chips to predict the composition. The results for the both types of CCDs are summarized in Table 3.

Caveat: The ECS data appear to be inconsistent with the line mixture from Table 3, see Fig. 2.

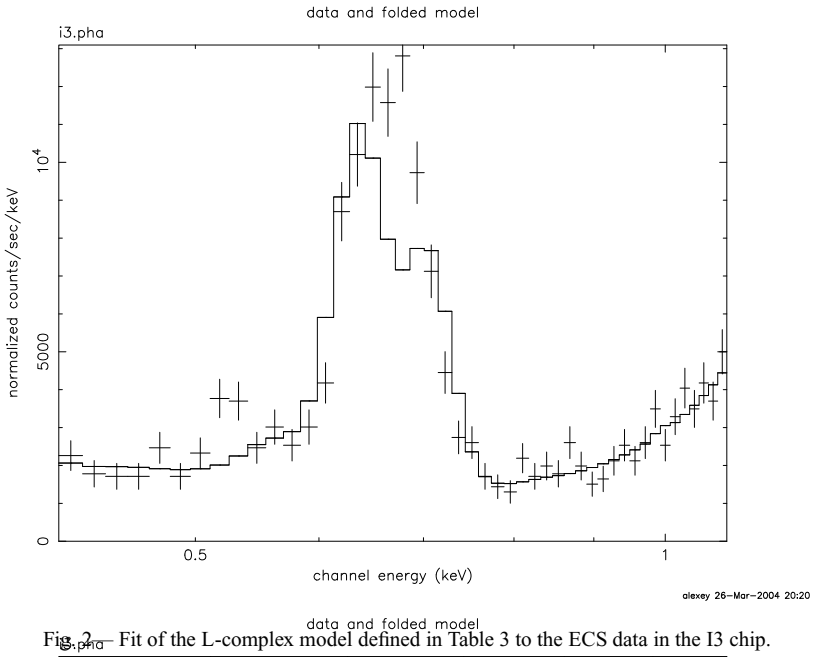

Fig. 2— Fit of the L-complex model defined in Table 3 to the ECS data in the I3 chip.

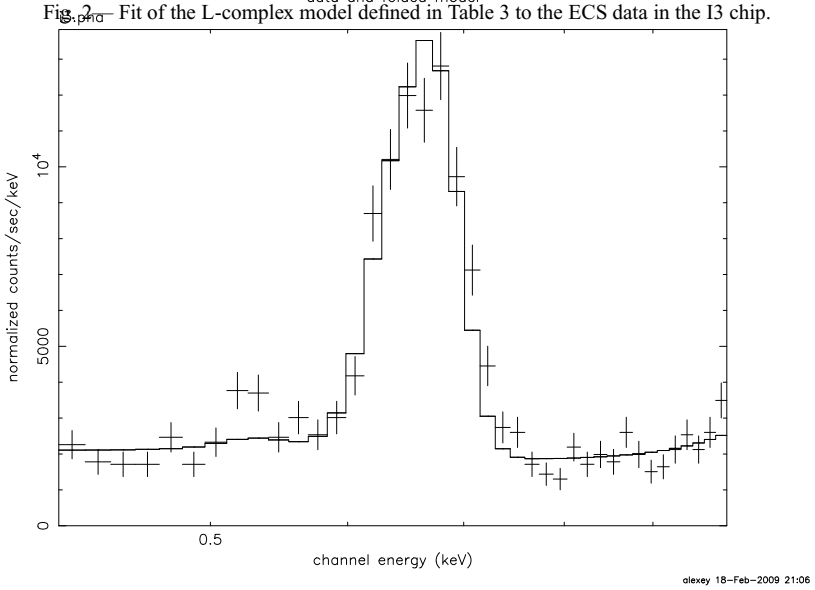

Fig. 3— Example of the L-complex fit with Mn + F lines.

Expected energy of the L-complex for the case of F-K line: Dan McCammon measured the flight spare of the ECS in 2008 and found no Fe-L line and instead an F-K line. Going over the same computation, we have

$$\langle E\rangle_{\text{Mn }\alpha,\beta} = 0.638\,\text{keV} \qquad \langle E\rangle_{\text{F-K}} = 0.679\,\text{keV}. \tag{3}$$

If X is the count rate fraction in F-K line, we can write the average energy of the L-complex as

$$\langle E\rangle = 0.679 \times X + 0.638 \times (1 - X) = 0.041\,X + 0.638. \tag{4}$$

Using the measurement $\langle E\rangle = 0.665$, we obtain **X = 0.66**. Therefore, the L-complex in the FI chips should consist of 34% in the Mn α,β lines, and 66% in F-K. Unlike the Mn+Fe lines model (Fig.2), the mixture of Mn and F lines provides a good fit to the data (Fig.3).

Correcting for the difference in QE for the two energies, the intrinsic ratio is 61:39. Eyeballing McCammon's spectra for the flight spare unit, the fluxes of the Mn and F lines are approximately equal. If this is due to aging of the source, we could predict

Table 3— Inferred composition of the ECS L-comlex

Line group	E, keV	f(FI)	EA(S3)	EA(S2)	S3/S2	f(BI)
Fe α,β	0.706	41%	0.628	0.324	1.938	35%
Mn α,β.....	0.638	57%	0.553	0.231	2.394	62%
Fe ζ,η	0.618	2%	0.528	0.202	2.601	3%
.....						
Mn ζ,η	0.559	$\sim 5\%$				$\sim 7\%$

Table 4— Inferred composition of the ECS L-comlex with F-K line

Line group	E, keV	f(FI)	EA(S3)	EA(S2)	S3/S2	f(BI)	f(intr)
F-K	0.679	66%	0.681	0.290	2.35	63%	61%
Mn α,β.....	0.638	34%	0.636	0.231	2.75	37%	39%

NOTE— QE for the S3 chips are different from those in Table 3 because they were taken in 1/2009 from an updated calibration file.

that the average energy for the S3 chip should evolve from 0.664 early on to 0.659 keV at present. This is a 0.8% change, marginally detectable at best.

3 Line Fluxes

Purpose: The ratio of the L-complex flux to the Mn-Ka line is used to monitor the ACIS contamination on-orbit. Also, the line flux ratios can be used for cross-calibration of the BI and FI CCDs.

Spectral model for the L-complex: It is clear from Figures 1 and 2 in §2 that the L-complex is more accurately fit by a single Gaussian (with free width) than by the mixture of the Mn and Fe lines listed in Table 3. Therefore, we use a single-Gaussian fit to derive the flux of the L-complex.

Note, however, the presense of the weak line to left of the main peak, near 0.53 keV (Fig. 1). It is visible in the spectral for all the FI CCDs in the Ball measurements, and also in the on-orbit data in the spectra extracted near the readout. This component does not interfere with the flux measurements from the Ball data because the high spectral resolution of the non-degraded FI CCD allows one to easily separate it from the main peak. However, in the flight data this line will be mixed with the main component because of the degraded spectral resolution, and this will bias the flux measurement. Experiments with the Ball data show that in all CCDs, this weak line has the same energy, 0.535 keV, and is consistent with the zero internal width and a total flux of 6.27% of the main peak (the average value for the flux measurements in the 5 FI CCDs). Therefore, the model of the L-complex consists of the following components:

1. Gaussian with free width at $E \approx 0.665$ (free) to represent the main peak
2. Gaussian line at $E = 0.535$ keV with zero width and the flux 0.0627 that of component 1.
3. Exponential tail representing the shoulder of the Al-Ka line.
4. Power law to model the background.

The fit is performed in the 0.3–1.2 keV band (PI channels 21–82). The results for I0–I3, S2, and S3 are shown in Fig. 4.

Spectral model for the main lines: The main lines in the ECS spectrum are modeled as 5 Gaussian component near 1.487 keV (Al-Ka), 4.510 keV (Ti-Ka), 4.930 keV (Ti-Kb), 5.898 keV (Mn-Ka), and 6.486 keV (Mn-Kb). The additional continuum (especially important in the S3 spectrum) is modeled as a power law with the high-energy exponential cutoff. To allow for small imperfections of the response model, we allow the line energies and widths to vary. This model provides a good fit the main peaks in the ECS spectrum. In the wings, there are small imperfections illustrated in Fig. 5:

1. The low-energy shoulders adjusted to fit the on-orbit ECS data in the FI chips appear to overpredict these components in the Ball spectra, especially in the Mn-Ka line. Note, however, that the total tail flux in this line is only 2.3%, so the inporrect models leads to only a $\sim 1.5\%$ bias in the line flux measurement.
2. The fluorescense peak in the FI model as a wrong energy. This is related to the algorithm used to rescale the FI RMFs (see §1).

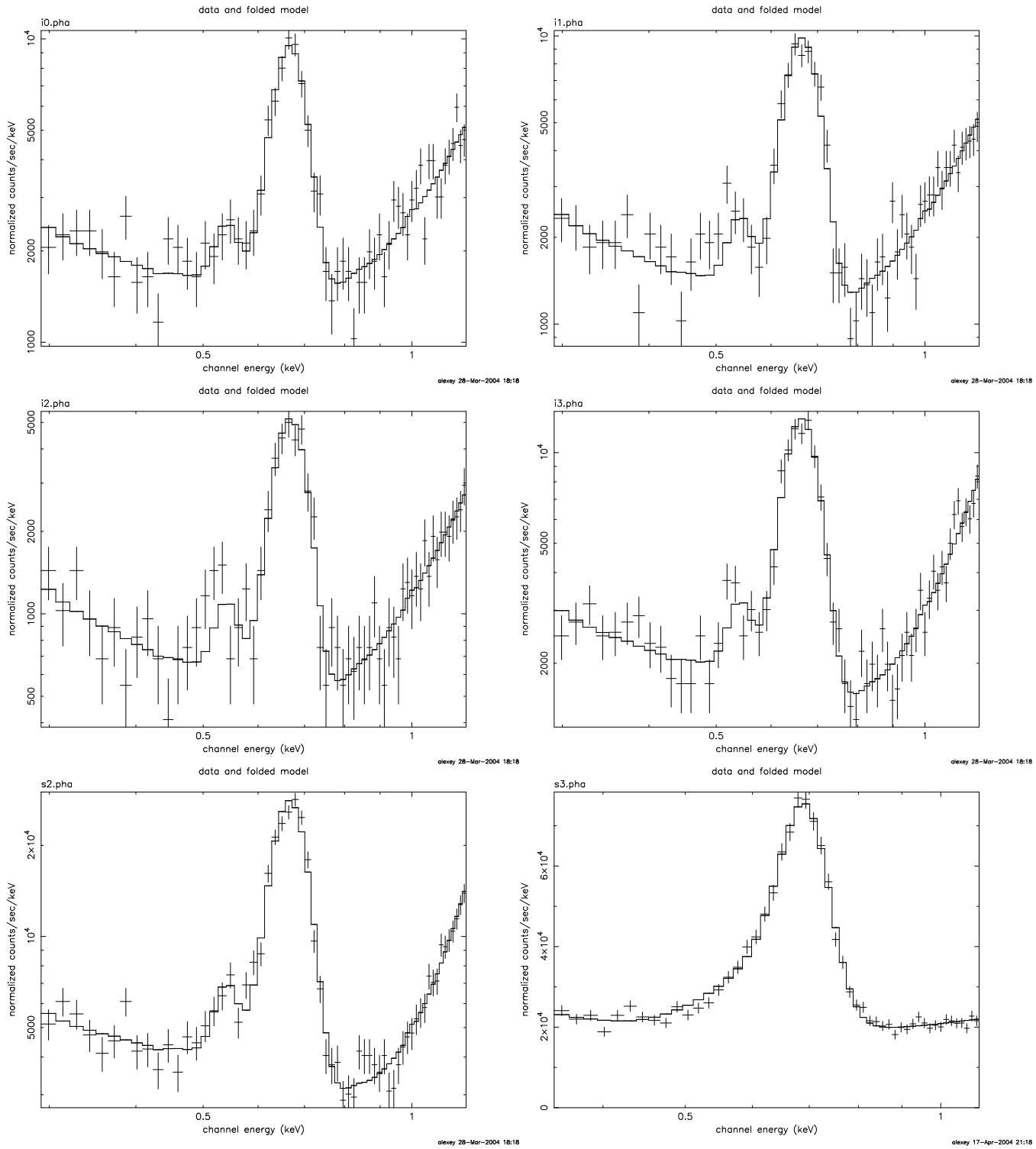

Fig. 4— Two-line fits to the L-complex in the I0–I3, S2, and S3 spectra

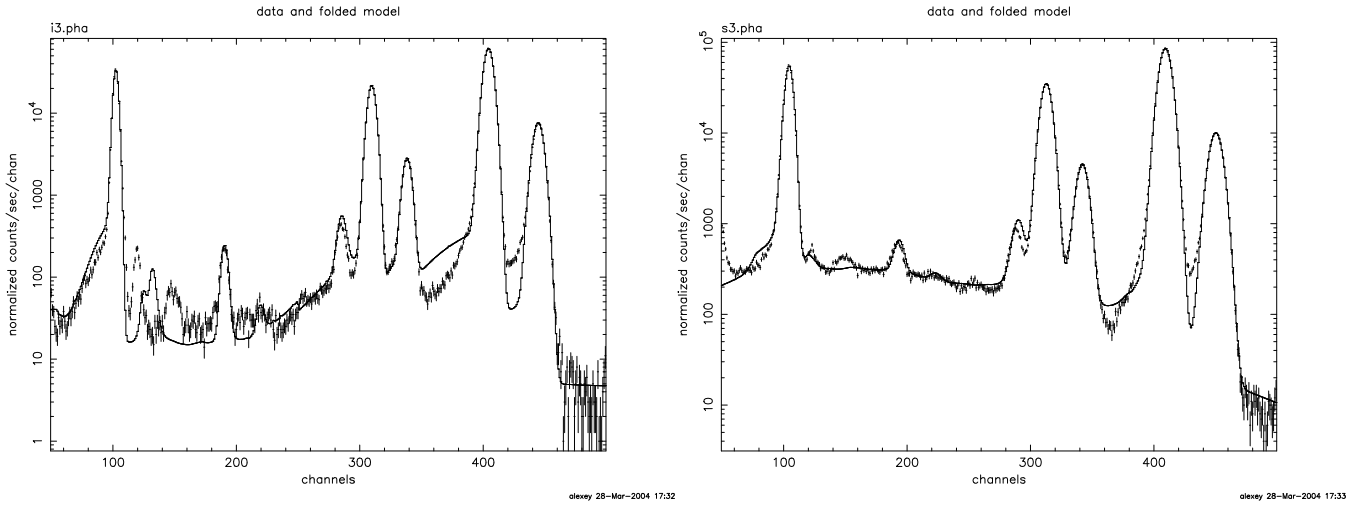

Fig. 5— Fits to the 5-Gaussian + continuum model to the ECS spectra in the full energy range for I3 (left) and S3 (right). The channel width is 14.6 eV.

3. Escape peaks may have slightly wrong energies/amplitudes.
4. There is a line complex near 2.1 keV not included in the model.
5. The region between the Mn-Ka and Kb lines is modeled incorrectly.

To minimize the biases in the main line flux measurements, we exclude the problematic regions from the fit.

The measured line fluxes for the L-complex and the 5 main lines are given in Table 5 on page 9.

3.1 Results

L-to-MnKa ratio. For the measurements of the contamination optical depth, we need the nominal value of the $\log(L/K)$ fluxes for Mn-Ka, corrected for quantum efficiencies etc. This is derived from the ECS measurements as

$$L/K = \frac{\text{L-flux} \times \text{QE}(5.898) \times \text{QEU}(5.898)}{\text{Mn-Ka-flux} \times \text{QE}(0.665) \times \text{QEU}(0.665)}. \quad (5)$$

Note that all FI chips had $\text{QEU}(E) = 1$ before they were radiation-damaged in flight. For the S3 chip, we assume that the QEU map calibrated on orbit applied also to the ground data. Using this equation, we measure **$\log(L/K) = -4.687$ for S3**, **$\log(L/K) = -4.925$ for the FI chips** (this ratio is the same for all FI chips within 5%), and **$\log(L/K) = -4.678$ for S1**.

Caveat: One would expect from eq. (5) that the L/K values should be the same in all CCDs. The observed difference between the FI chips and S3 is much larger than the uncertainties; most likely it is explained by an error in the cross-calibration of the CCD QE.

L-to-MnKa ratio for the multi-line model including F-K. Equation (5) ignores that the L-complex is not a single line. A more accurate expression is

$$L/K = \frac{\text{L-flux} \times \text{QE}(5.898) \times \text{QEU}(5.898)}{\text{Mn-Ka-flux} \times (0.39\,\text{QE}(0.638) + 0.61\,\text{QE}(0.679)) \times \text{QEU}(0.665)}. \quad (6)$$

With this equation, **$\log(L/K) = -4.754$ for S3**.

Cross-calibration of the quantum efficiencies in S2 and S3. Since the illumination patterns in the S2 and S3 chips are the same (§4), we can use the derived absolute line fluxes to cross-calibrate the CCD QE. The absolute line flux, f, is defined as

$$f = \frac{\text{Observed flux}}{\text{exposure} \times \text{QE} \times \text{QEU}}. \quad (7)$$

The results for the absolute fluxes are reported in Table 6. The agreement between the absolute fluxes — especially after the 3/2004 MIT correction — is good, within 2%. This is probably within the uncertainties related to the RMF model.

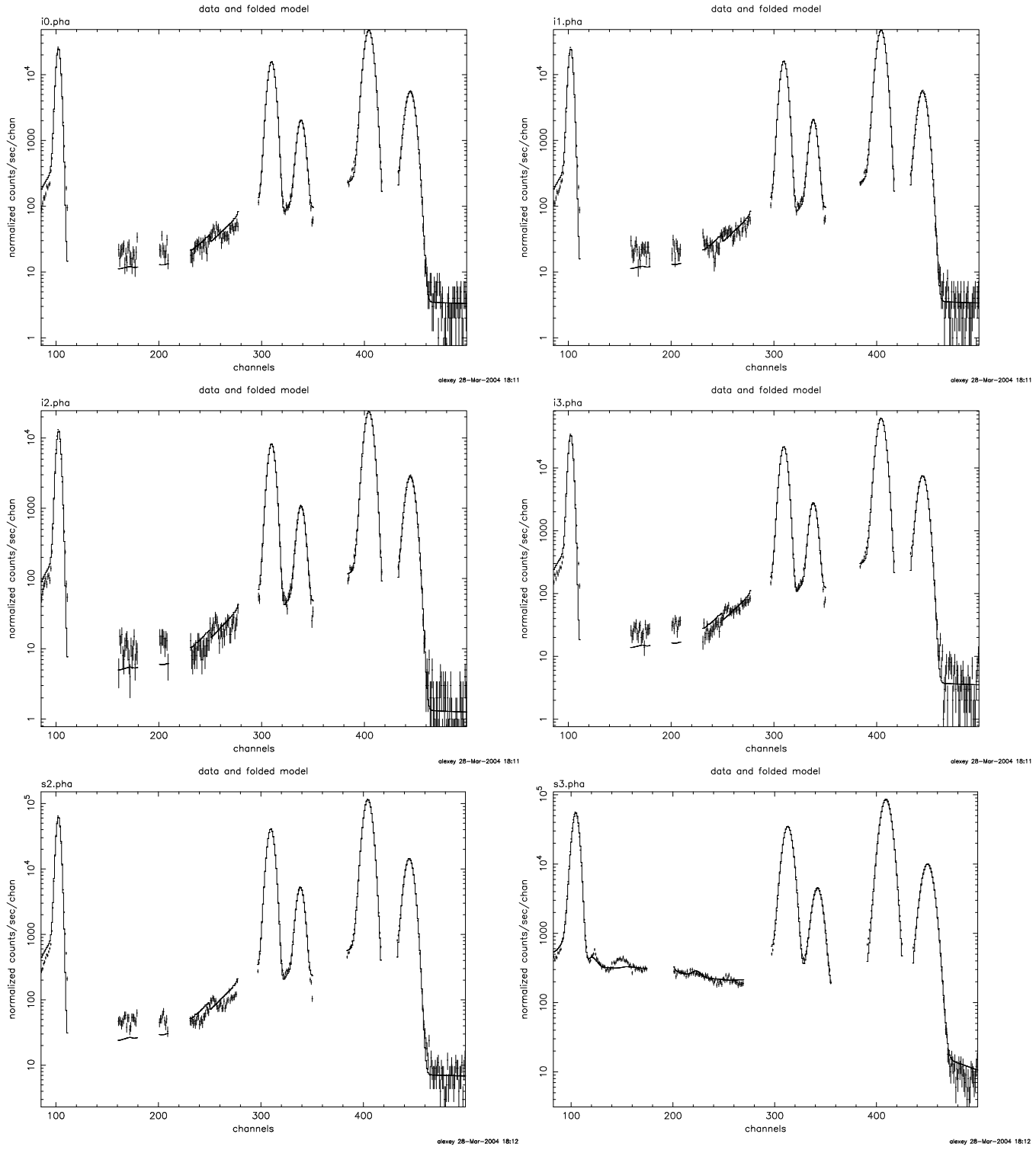

Fig. 6— Five-line plus continuum fits to the high energy part of the ECS spectrum in I0–I3, S2, and S3.

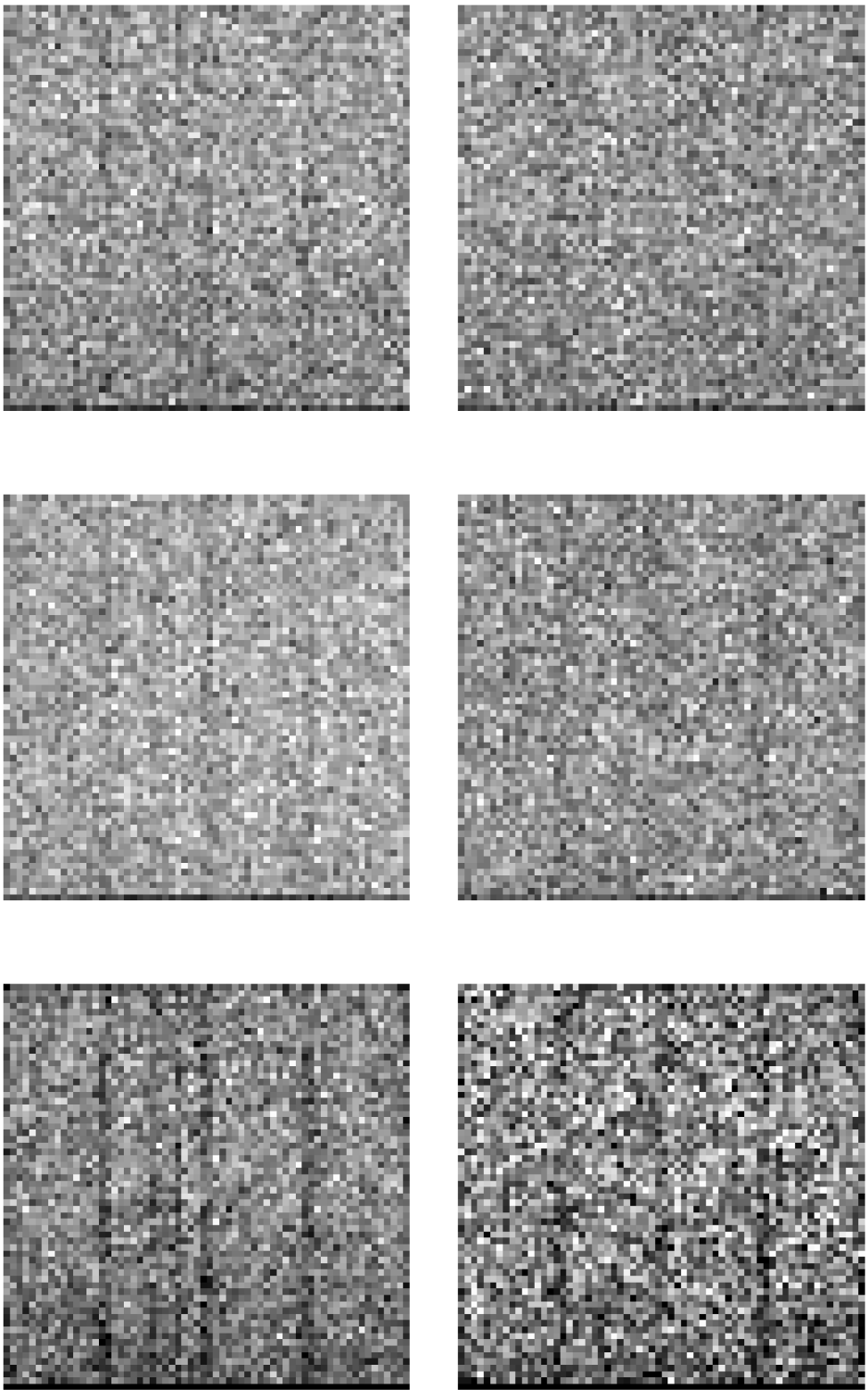

Fig. 7— Images of the S2 and S4 chips (left and right, respectively), in the Al, Ti, and Mn lines (top to bottom).

Table 5— ECS line fluxes in the Ball data

	Line flux, cnts							Nominal QE (CCD+filter)				Average QEU			
CCD	L*	Al-Ka	Ti-Ka	Ti-Kb	Mn-Ka	Mn-Kb	t_{exp}, s	0.665	1.487	4.510	5.898	0.665	1.487	4.510	5.898
I0	729.0	132352	131279	17129	460821	60581	4973	0.202	0.819	0.937	0.871	1.000	1.000	1.000	1.000
I1	809.8	133007	133285	17139	460608	60627	4973	0.206	0.821	0.937	0.871	1.000	1.000	1.000	1.000
I2	413.4	67632	68374	9040	232999	30978	2485	0.216	0.826	0.939	0.872	1.000	1.000	1.000	1.000
I3	1088.5	176360	182155	23449	598472	80124	6450	0.206	0.821	0.937	0.871	1.000	1.000	1.000	1.000
S2	2412.9	330983	342502	44476	1122630	153285	11780	0.270	0.849	0.949	0.908	1.000	1.000	1.000	1.000
S3	8132.0	437383	392889	51439	1056967	135049	14165	0.584	0.926	0.938	0.752	0.996	0.981	0.943	0.929
S1	2794.3	139566	105782	13696	291524	36127	4846	0.584	0.911	0.878	0.644	0.982	0.942	0.879	0.864

* For the L-complex we report the flux of the main Gaussian component. The total flux is a factor of 1.0627 higher (see p. 4).

Table 6— Comparison of the absolute fluxes in S2 and S3

	Absolute line flux[a]		
CCD	Al-Ka	Ti-Ka	Mn-Ka
S2	33.083	30.630	105.007
S3	33.981	31.430	107.027
S3/S2	1.027	1.026	1.019
3/25/04 correction[b]	1.025	1.007	1.004

[a] Absolute line fluxes were derived from the measured intensities reported in Table 5 using equation (7).
[b] QE correction from MIT in March, 2004

4 Illumination pattern

The illumination pattern of ECS on ACIS must be taken into account in the measurements of the quantum efficiency non-uniformities (QEU) using the spatial distribution of the line intensities in the on-orbit data. Since the FI CCDs were intrinsically uniform on the ground, the illumination pattern can be established simply from the spatial distribution of intensities in the Ball data. We do this separately for ACIS-S and ACIS-I.

Data preparation The illumination analysis was performed using the chip images in the energy ranges corresponding to the main ECS lines. The images were extracted in the chip coordinates in the PI channel ranges 70–118, 3000-365, and 380–480 for the Al, Ti, and Mn lines, respectively. Note the for the Ti and Mn lines, our energy bands include both Ka and Kb lines (Fig. 6).

4.1 ACIS-S

The CCDs of most interest are S1–S4. We will demonstrate that the illumination patterns are the same in S2 and S4 (it is a function of `CHIPY` and constant along `CHIPX`). Therefore, the S2 pattern should apply also to the S3 chip.

Results The images of the S2 and S4 CCDs in the Al, Ti, and Mn lines are shown in Fig. 7. The only visible non-uniformities are along the Y direction and there is no obvious X-dependence. This is better illustrated by the projections to the `CHIPY` and `CHIPX` axis shown in Fig. 8. While there are strong gradients of intensity along the `CHIPY` direction, especially, for the Al and Mn lines, the X-projections are essentially flat. Therefore, we assume that there is no `CHIPX` dependence of the illumination pattern for the S2 and S4 — and therefore, S3 — CCDs. The `CHIPY`-dependence was fit to a function in the form

Table 7— ECS line fluxes in the adjacent regions in S2 and S3

	S3			S2			Flux			
E, keV	I, cnt	QE×U	t_{exp}, s	I, cnt	QE	t_{exp}, s	S3	S2	S3/S2	3/25/04 correction
1.487 ..	25626	0.9236	14165	19316	0.8493	11780	1.960	1.931	1.0152	1.025
4.510 ..	24570	0.9262	14165	20567	0.9492	11780	1.870	1.839	1.0169	1.007
5.898 ..	66314	0.7418	14165	65190	0.9075	11780	6.312	6.098	1.0351	1.004

$I^{-1} = 1 + ((y - y_0)^2/\Delta^2)^\alpha$. The best fit relations for the Al, Ti, and Mn lines,

$$
\begin{aligned}
I &= \left[1 + \left((y - 910)^2/1900^2\right)^{1.5}\right]^{-1} \qquad \text{(Al)} \\
I &= \left[1 + \left((y - 550)^2/1100^2\right)^{2.0}\right]^{-1} \qquad \text{(Ti)} \\
I &= \left[1 + \left((y - 690)^2/3600^2\right)^{1.0}\right]^{-2} \qquad \text{(Mn),}
\end{aligned}
\tag{8}
$$

are shown by the red lines in Fig. 8 [*yes, the outer index is* -2 *for Mn*].

4.2 ACIS-I

Image normalizations. The line intensity gradients in ACIS-I have very large scale and are best-modeled for the array as a whole and therefore, the images for the individual CCDs must be properly normalized. We use the average line intensities in the squares of 384×384 adjacent to the center of ACIS-I for normalization.

The normalized images are shown in Fig. 9. There are detectable intensity gradients across ACIS-I, especially for the Ti line. We fit the combined images with the two-dimensional polynomial of the second order in the Y-direction (perpendicular to ACIS-S), and first order in the X-direction. The results are shown in Fig. 10. The illumination variations are small, within ±5% for all lines. Note that our QEU analysis will rely on the intensity of the Mn lines which has the higher statistics and fortunately, a virtually flat illumination map.

The combined illumination model for ACIS-I and ACIS-S can be found in
`/data/alexey3/chandra3/CAL/ECS.illum.fits.gz`

5 Further cross-calibration of the QE in S2 and S3

To minimize the effects of the illumination variations and QEU, we extracted the spectra from the adjacent regions near the readout of S3 and S2 (defined as `CHIPY` $= 10 - 256$, `CHIPX` $= 2 - 255$ for S3 and `CHIPX` $= 771 - 1023$ for S2. The added benefit is the higher spectral resolution in this region so the line fluxes can be measured with less systematic uncertainty. The results for the main lines are reported in Table 7. If the CCD QE model for S2 is correct, these results favor a mild increase of the QE for the S3 chip at high energies. The systematic uncertainty in these measurements is estimated to be 1.5%.

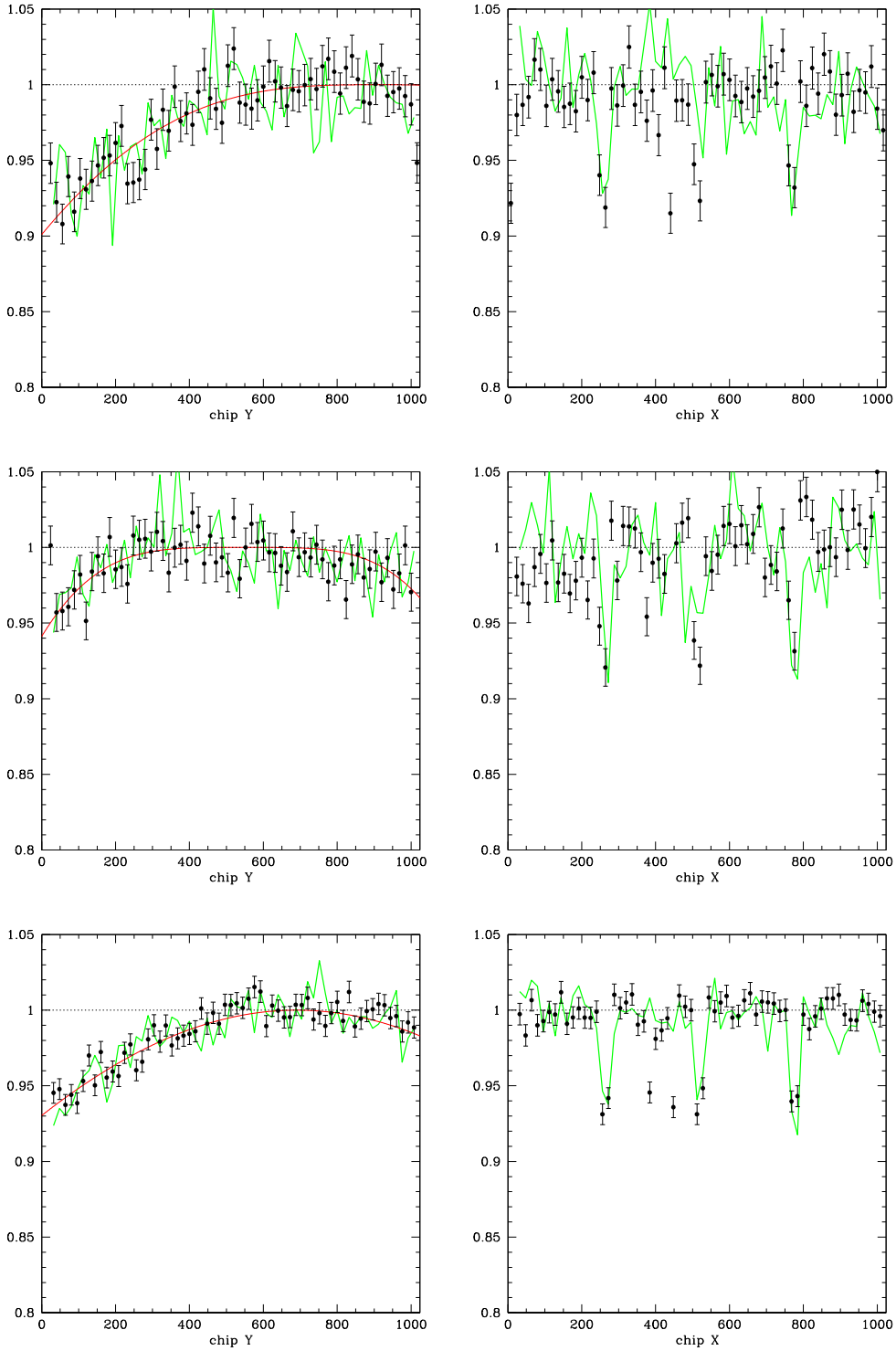

Fig. 8— Projections of the S2 and S4 images in Al, Ti, and Mn (top to bottom) to the CHIPY and CHIPX axis (left and right, respectively). The data for S2 are shown by the black points with the errorbars and the S4 profile is shown by the green line. Red lines in the CHIPY plots show the best fit by equation (8). A small number of strong negative deviations in the CHIPX plots are caused by the presence of bad columns.

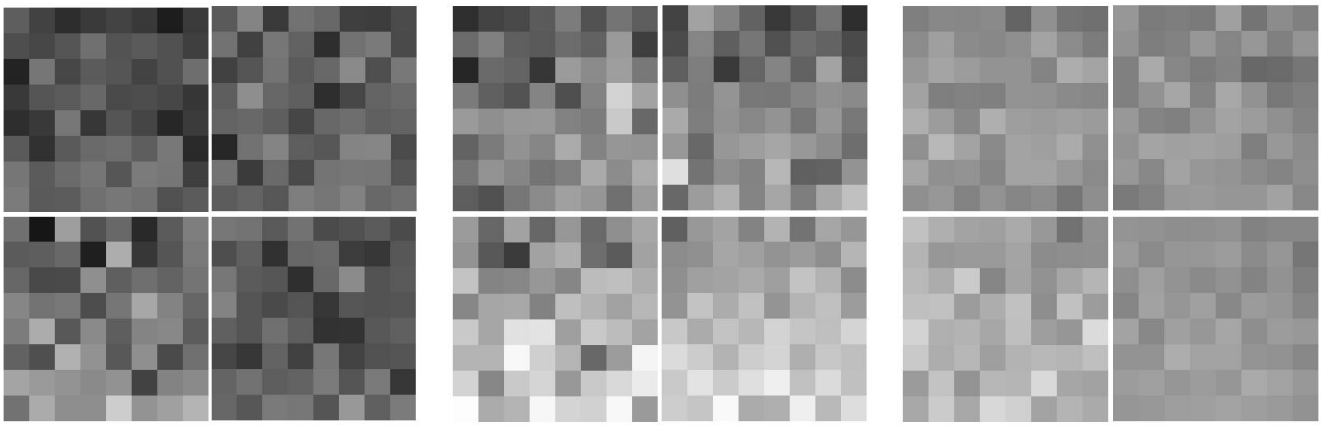

Fig. 9— Images of ACIS-I in the Al, Ti, and Mn lines (left to right). Orientation is as in the "ACIS FLIGHT FOCAL PLANE" figure from the Observatory guide: I0 is on the top-left, I3 is on the bottom-right. The color range is ±10% in each panel.

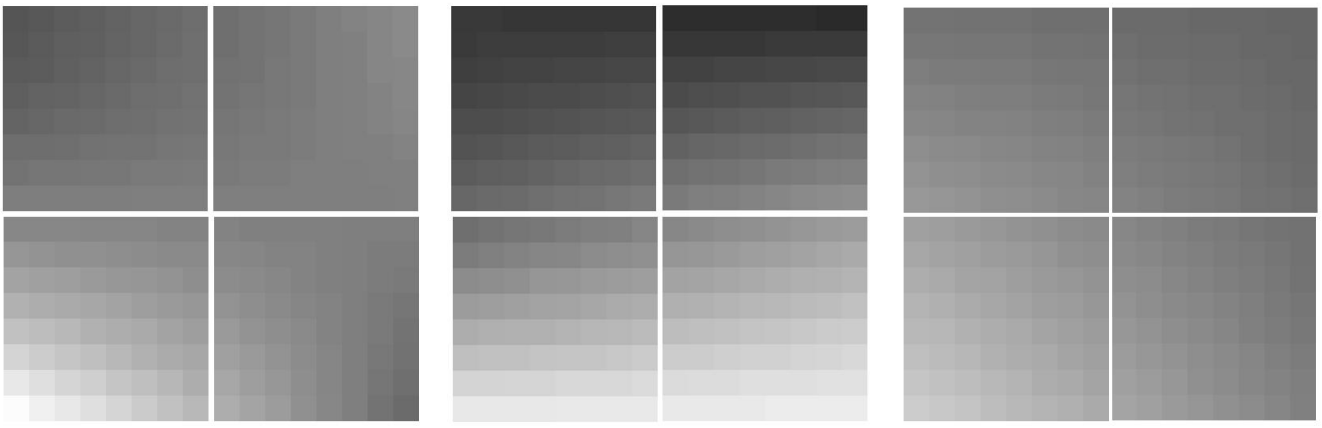

Fig. 10— Best-fit illumination patterns of ACIS-I in the Al, Ti, and Mn lines (left to right). Orientation is the same as in Fig. 9. The color range is ±10% in each panel. The intensity variations are within ±5% for all lines.